Journal of Materials Chemistry A

COMMUNICATION

Cite this: J. Mater. Chem. A, 2017, 5, 1406

Received 4th December 2016
Accepted 13th December 2016

DOI: 10.1039/c6ta10418e

www.rsc.org/MaterialsA

A TiO_2 embedded structure for perovskite solar cells with anomalous grain growth and effective electron extraction†

Dong Wei,[a] Jun Ji,[a] Dandan Song,[a] Meicheng Li,*[ab] Peng Cui,[a] Yaoyao Li,[a] Joseph Michel Mbengue,[a] Wenjia Zhou,[c] Zhijun Ning[c] and Nam-Gyu Park[d]

The structure of the perovskite solar cells (PSCs) is either mesoporous or planar. Here, a novel structure for highly efficient and stable PSCs is proposed, *i.e.*, an embedded structure, which combines the advantages of the mesoporous and planar structures. The embedded structure utilizes a TiO_2 nanoparticle embedded perovskite ($CH_3NH_3PbI_3$) film as the absorption layer. The presence of TiO_2 nanoparticles in the perovskite film could improve the electron extraction, and promote the formation of a compact perovskite layer with large grains. Consequently, the performance of the PSCs is significantly improved with the efficiency increasing from 16.6% for the planar structure to 19.2% for the embedded structure, which is the best performance of the $MAPbI_3$-based PSCs. Furthermore, the TiO_2 embedded perovskite films present better long-term stability than the pristine perovskite films, and the corresponding PSCs, which have no other chemical modifications, also show excellent stability with efficiency approaching 80% (for average) or 90% (for the best) after being exposed to air for 28 days without encapsulation.

Introduction

Organic–inorganic halide perovskite solar cells (PSCs) possess the advantages of low-cost and high performance, especially the power conversion efficiency (PCE).[1–6] The outstanding performance of the PSCs relies both on the perovskite itself and the device structure. The structure of the PSCs is either mesoporous or planar, depending on the presence or absence of a mesoporous scaffold layer.[7,8]

In PSCs with a mesoporous structure, the mesoporous layer employs a mesoporous oxide (TiO_2 or Al_2O_3) scaffold layer filled with perovskite grains. Typically, in the TiO_2-based mesoporous structure, photo-induced electrons generated from perovskite are demonstrated to be collected and transported by the TiO_2 scaffold.[5] However, it is also proved that the presence of the TiO_2 mesoporous layer increases the series resistance of the PSCs, due to the inhibiting effect on the growth of perovskite grains and the lower charge transport efficiency in the mesoporous layer with respect to perovskite itself,[9,10] leading to lower device performance compared to the PSCs based on the planar structure. In addition, mesoporous PSCs usually require a high temperature annealing process for the formation of a high-quality TiO_2 scaffold layer to reduce the interfacial recombination between the TiO_2 scaffold layer and the perovskite layer.[11]

In contrast, the planar structure employs a pristine perovskite layer directly deposited on the compact layer, which shows unique performance for efficient PSCs on the basis of the ambipolar nature of the perovskite material,[12] avoiding additional series resistance and other disadvantages caused by the mesoporous layer. Moreover, this structure can be facilely fabricated at low temperature. However, it is shown that planar PSCs suffered relatively low long-term stability compared to the mesoporous PSCs,[13] because of the electron recombination at the perovskite/compact layer interface and the shunting paths resulting from the presence of pin-holes in the perovskite film resulting from the absence of the TiO_2 mesoporous layer. Hence, the electron-conducting TiO_2 is indispensable, at least to some extent, for highly performing and long-term stable PSCs, and it is crucial to explore solutions to avoid its weakness.

In this work, we propose a facile method to take advantage of TiO_2 overcoming its obstacles, which enables the high efficiency and long-term stability of the as-prepared PSCs. The TiO_2 embedded structure, instead of the traditional TiO_2 mesoporous structure, is explored by incorporating TiO_2 nanoparticles into perovskite grains (instead of filling TiO_2 pores with perovskite grains). The TiO_2 embedded structure could provide an efficient pathway for electron extraction and avoid

[a]State Key Laboratory of Alternate Electrical Power System with Renewable Energy Sources, School of Renewable Energy, North China Electric Power University, Beijing 102206, China. E-mail: mcli@ncepu.edu.cn; Fax: +86 10 6177 2951; Tel: +86 10 6177 2951

[b]Chongqing Materials Research Institute, Chongqing 400707, China

[c]School of Physical Science and Technology, ShanghaiTech University, Shanghai 201210, China

[d]School of Chemical Engineering, Sungkyunkwan University, Suwon 440-746, Korea

† Electronic supplementary information (ESI) available. See DOI: 10.1039/c6ta10418e

the unfavorable resistance induced by the massive interfaces of TiO_2 mesoporous layers. Furthermore, the embedded TiO_2 could promote the grain growth of perovskite to form a large-grain compact perovskite film. Meanwhile, a two-step mechanism for the anomalous grain growth is revealed. The average PCE of such PSCs with the TiO_2 embedded structure (embedded PSCs) improved compared to that of the standard planar PSCs, from 16% to 18%, and the highest efficiency of embedded PSCs achieved was 19.2%, which is the best performance of the $CH_3NH_3PbI_3$-based PSCs. More encouragingly, the embedded PSCs exhibit notable long-term air stability, which keeps approaching 80% of their original efficiency after being exposed to air for 28 days. In contrast, the standard planar structure PSCs showed marked degradation (almost 40%) after being exposed for the same period.

Results and discussion

The schematic illustration of PSCs with different structures is shown in Fig. 1. As shown in Fig. 1a, the mesoporous PSCs have a mesoporous layer infiltrated with perovskite and a perovskite capping layer together acting as the light absorption layer. The mesoporous layer extracts and transfers photo-induced electrons from perovskite. Consequently the performance of the device is closely bounded up with its thickness and porosity. Different from the mesoporous PSCs, the planar PSCs possess a pristine perovskite layer, as shown in Fig. 1b, which forms the heterojunction with the n-type compact layer directly. The photo-induced electrons could be selected and transferred at the interface of the compact TiO_2 layer and the perovskite layer. Distinct from those two standard structures, the embedded PSCs, as shown in Fig. 1c, have a hybrid absorption layer with the well-defined TiO_2 nanoparticles embedded uniformly into the perovskite grains. These TiO_2 nanoparticles surround the perovskite grains and form electron transport pathways from the perovskite layer to the compact TiO_2 layer. As the result, the photo-induced electrons can be extracted by the nearest TiO_2 nanoparticles and transported by the embedded TiO_2 network efficiently. Hence, this TiO_2 embedded structure simultaneously favors the electron extraction in PSCs and provides a discontinuous scaffold structure for better stability of perovskite films.

The TiO_2 embedded perovskite film was obtained *via* spin coating TiO_2/PbI_2 solution on the compact layer followed by dipping into MAI (MA = CH_3NH_3) solution to form the perovskite ($MAPbI_3$) film.[14] Here, different amounts of TiO_2 are introduced by varying the content of TiO_2 while fixing the PbI_2 concentration in the solution, which is 0–0.1 wt% in the TiO_2/PbI_2 blend.

The representative current density–voltage (J–V) curves of the PSCs prepared from different TiO_2 amounts in the TiO_2/PbI_2 blend are shown in Fig. 2. The average results of photovoltaic parameters obtained from twenty corresponding PSCs including short-circuit current density (J_{SC}), open-circuit voltage (V_{OC}), fill factor (FF) and photoelectric conversion efficiency (PCE) are summarized in Table 1. It can be seen that the performance of the PSCs prepared from x wt% ($x > 0$) TiO_2 in the TiO_2/PbI_2 blend (defined as embedded PSCs) presents an increase–decrease trend in device performance, especially in J_{SC}, FF and PCE, indicating that the presence of TiO_2 nanoparticles in perovskite, despite their trace amount, has a significant influence on the performance of PSCs. A significant improvement of device performance is shown by the embedded PSCs under the condition of 0.05 wt% TiO_2, which exhibits a PCE of 18.93% (10% higher than that of the standard planar PSCs). When the TiO_2 amount was lower than 0.05 wt%, the embedded PSCs perform similarly to the standard planar ones, as the TiO_2 nanoparticles are not able to affect the device performance by a large extent with a low wt%. It is worth noting that the FFs of the embedded PSCs prepared under the conditions of 0.03–0.05 wt% TiO_2 are higher than that of the standard planar PSC, which implies that the series resistance is reduced

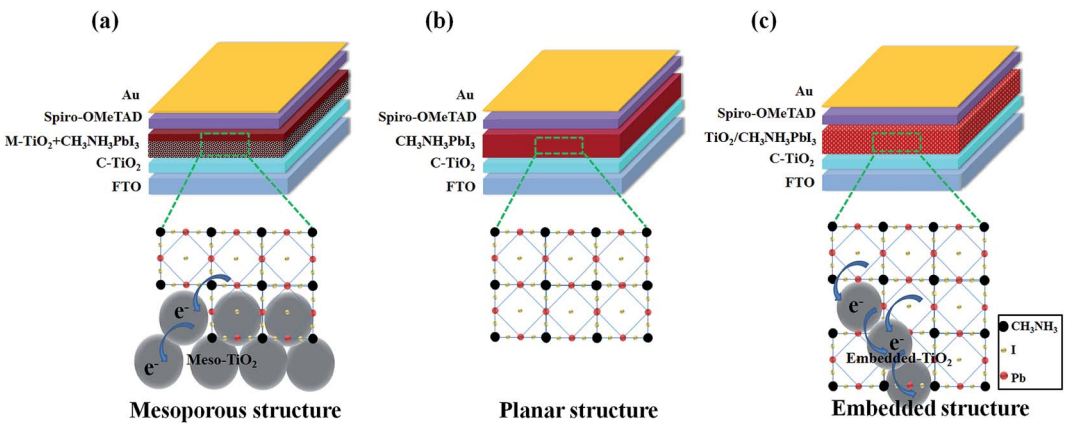

Fig. 1 Schematic illustration of the structure and the electron transfer of perovskite solar cells: (a) mesoporous structure employing a thin TiO_2 mesoporous layer (M-TiO_2), which could extract and transfer photo-induced electrons. (b) Planar structure with a well-crystallized pristine perovskite layer deposited directly on the compact TiO_2 (C-TiO_2) layer, which acts as the electron-extractive layer. (c) TiO_2 embedded structure involving a TiO_2 embedded perovskite layer, which could achieve more efficient extraction and transfer of electrons between TiO_2 and perovskite.

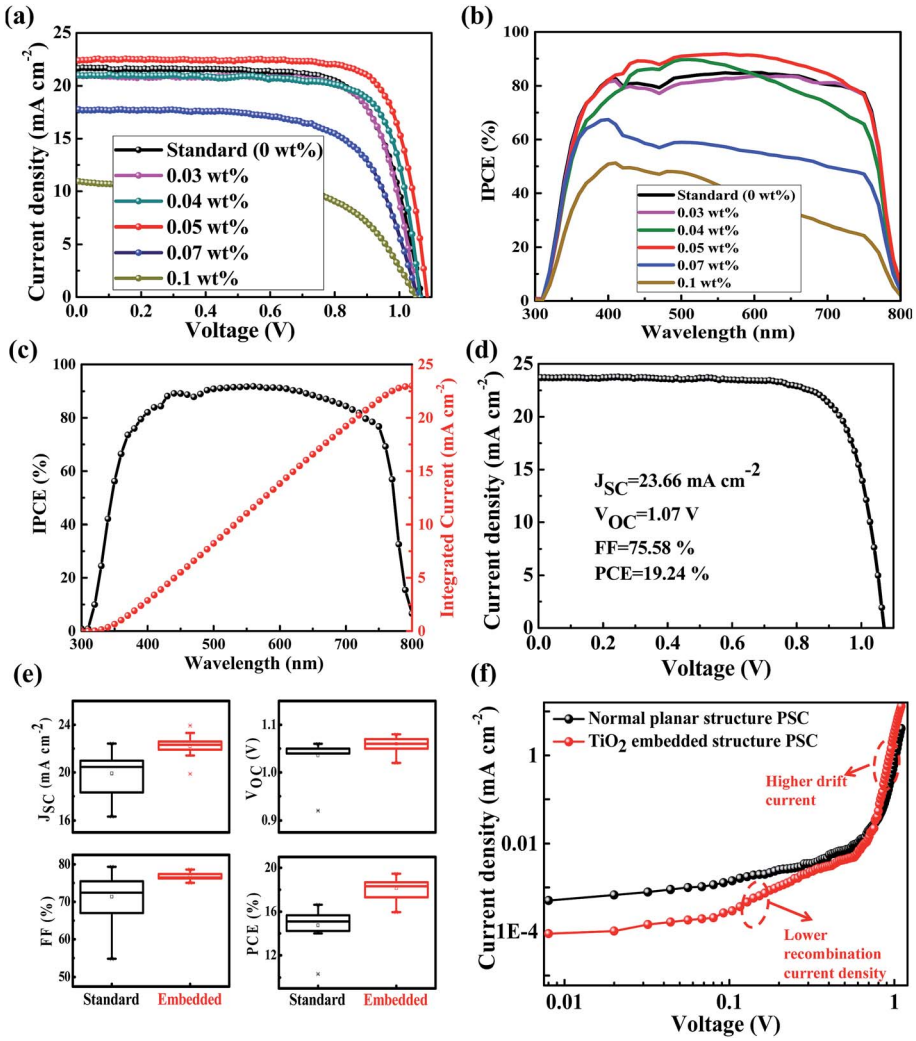

Fig. 2 (a) Current density–voltage (J–V) curves obtained for the PSCs fabricated with different TiO_2 amounts in the TiO_2/PbI_2 blend (0–0.1 wt%). All the PSCs were measured under AM 1.5G solar irradiation of 100 mW cm^{-2} in ambient atmosphere without encapsulation at a constant rate of 100 mV s^{-1}. (b) IPCE curves of PSCs with different TiO_2 amounts in the TiO_2/PbI_2 blend. (c) IPCE of the embedded PSC (0.05 wt% TiO_2) and the corresponding integrated current that is generated under AM 1.5G irradiation. (d) J–V curve measured for the best-performing embedded PSCs. (e) Average values of J_{SC}, V_{OC}, FF and PCE obtained for the standard planar PSCs and the TiO_2 embedded PSCs. Error bars indicate the standard deviation; twenty devices per type were used. (f) log–log plots of dark J–V curves of PSCs with the planar structure and the TiO_2 embedded structure.

Table 1 Photovoltaic parameters of the PSCs prepared from different TiO_2 amounts in the TiO_2/PbI_2 blend (0–0.1 wt%)

Amounts of TiO_2 nanoparticles	J_{SC} (mA cm^{-2})	V_{OC} (V)	FF (%)	PCE (%)
Standard (0 wt%)	21.57	1.06	72.44	16.62
0.03 wt%	20.97	1.05	75.29	16.61
0.04 wt%	21.02	1.06	75.85	16.96
0.05 wt%	22.40	1.08	77.70	18.93
0.07 wt%	17.88	1.05	65.0	12.39
0.1 wt%	11.05	1.05	62.0	7.31

by introducing TiO_2 nanoparticles in perovskite. When the amount of TiO_2 nanoparticles (0.07–0.1 wt%) is further increased, the device performance becomes poorer than that of the standard planar PSCs. IPCE (incident photon-to-electron conversion efficiency) spectra of the PSCs presented in Fig. 2b show the same trend in the change of the IPCE as that of the J_{SC} obtained from J–V curves (listed in Table 1). The highest IPCE is also obtained under the condition of 0.05 wt% TiO_2, leading to a J_{SC} of 22.9 mA cm^{-2} calculated from the IPCE spectrum (as shown in Fig. 2c), which is similar to the result obtained by J–V measurements. The poor performance of the embedded PSCs prepared from a large amount of TiO_2 nanoparticles is caused by the increased series resistance in the perovskite film induced by the high density of TiO_2 nanoparticles in the perovskite film, leading to the lowered J_{SC}, FF and the resultant PCE.

The highest efficiency achieved by the embedded PSCs is 19.2% (as shown in Fig. 2d), in which the perovskite film is prepared from 0.05 wt% TiO_2 in the TiO_2/PbI_2 blend. Moreover,

the average performance of the embedded PSCs (0.05 wt% TiO_2) is obviously better than that of the standard planar PSCs. As can be seen in Fig. 2e, the average values of J_{SC}, V_{OC}, FF and PCE corresponding to the embedded PSCs present an excellent reproducibility compared to that of the standard planar PSCs. The average PCE of the embedded PSCs is improved by 10% compared to that of the standard planar PSCs.

Dark *J–V* characteristics of the planar and embedded PSCs are analyzed to get a further insight into the role of the TiO_2 in the device performance.[15] As shown in Fig. 2f, the dark current density is composed of the recombination current in the space charge zone at low voltages and the drift current across the device at high voltages. The embedded PSC displays a lower recombination current density and a higher drift current than the planar PSC. These phenomena indicate that the recombination in the space charge zone is reduced by incorporating TiO_2 in perovskite. In addition, the electrical parameters including the reverse saturation current (J_0) and the series resistance (R_s) of the PSCs with and without TiO_2 were calculated by fitting dark *J–V* curves using the Shockley equation:

$$J = J_0\left[\exp\frac{-q(V - AJR_s)}{mk_BT} - 1\right] + \frac{V - AJR_s}{AR_{sh}} \quad (1)$$

where A and m represent the device area and the diode ideality factor, R_{sh} represents the shunt resistance, respectively. Dark curves of the standard planar and the TiO_2 embedded PSCs and the corresponding curves fitted by eqn (1) are shown in Fig. 3. As J_0 is determined by the carrier recombination induced by trap states, lower J_0 (3.72×10^{-6} mA cm^{-2}) of the embedded PSC reveals lowered carrier recombination and reduced trap states in the presence of TiO_2 nanoparticles in the perovskite film than the standard PSC ($J_0 = 1.03 \times 10^{-5}$ mA cm^{-2}). Furthermore, the value of R_s (5.8 Ω) is lower in the embedded PSC than in the planar PSC (R_s = 35.62 Ω), which indicates that the carrier transport is more favorable in the embedded PSC. The reduced carrier recombination and lowered series resistance are beneficial for a higher J_{SC} and FF of the PSCs; therefore, the embedded PSCs exhibit high device performance than the planar PSCs.

From the above *J–V* characteristic analysis, it is clear that the incorporation of TiO_2 nanoparticles in fabricating the perovskite film has significant impact on the device performance. Theoretically, the TiO_2 nanoparticles probably function through two aspects. One is the engineering of the perovskite film during fabrication. The other one is their electronic properties, which are similar to their role in mesoporous PSCs, *i.e.*, the electron extraction and electron transport properties.

To investigate the morphological properties of the TiO_2 embedded perovskite film, scanning electron microscopy (SEM) images of the perovskite films with different amounts of TiO_2 in the TiO_2/PbI_2 blend (0.03–0.1 wt%) were recorded and shown in Fig. S1.† The TiO_2 embedded perovskite films with various TiO_2 amounts are all more compact with a larger grain size than the pristine perovskite film. In particular under the condition of 0.05 wt% TiO_2 in the TiO_2/PbI_2 blend, the grain size is obviously larger in the embedded perovskite film than in the pristine perovskite film, as shown in the SEM images in Fig. 4a and c. The pristine perovskite film yields a poly-crystalline morphology with a grain size of around 200 nm, whereas the embedded perovskite film exhibits an average grain size of 800 nm along with a more preferred orientation as confirmed from the layered morphology. Furthermore, the embedded perovskite film is more uniform and dense. Thus it is clear that the mechanisms of grain growth of the perovskite films with and without TiO_2 are quite different. This anomalous phenomenon of grain growth of the embedded perovskite film involves two kinetic processes: the fast heterogeneous nucleation process[16] and the anomalous grain growth mechanism.[17,18]

At the nucleation stage, TiO_2 nanoparticles dispersed in the precursor solution provide many heterogeneous nucleation sites which facilitate the nucleation of perovskite, owing to the lower nucleation energy barrier at the heterogeneous TiO_2/PbI_2 solution interfaces than at the homogeneous interfaces.[19] Hence, the heterogeneous nucleation process induced by the embedded TiO_2 nanoparticles promotes the nucleation of perovskite grains, as depicted in Fig. 4b and d, which makes the as-prepared perovskite film more compact. Meanwhile, the embedded TiO_2 nanoparticles provide many nucleation sites,

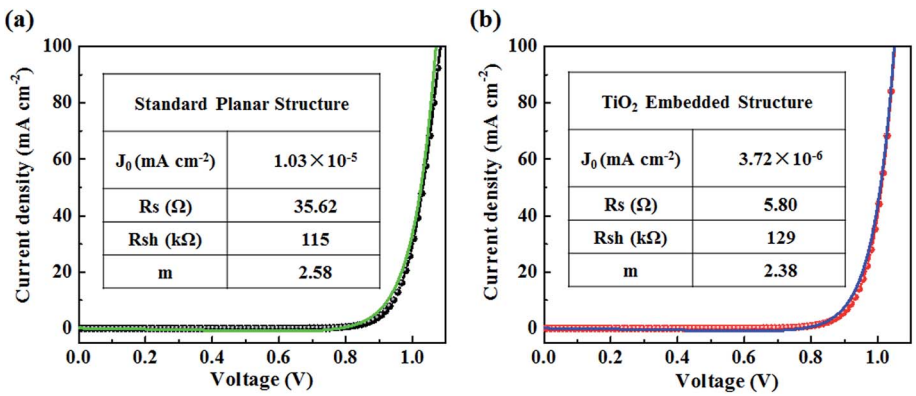

Fig. 3 Dark curves and the fitting curves of (a) the standard planar PSC and (b) the TiO_2 embedded PSC. Inside parameters are calculated by fitting dark curves corresponding to the standard planar and the TiO_2 embedded PSCs. Lower J_0 of the TiO_2 embedded PSC reveals lowered carrier recombination and reduced trap states.

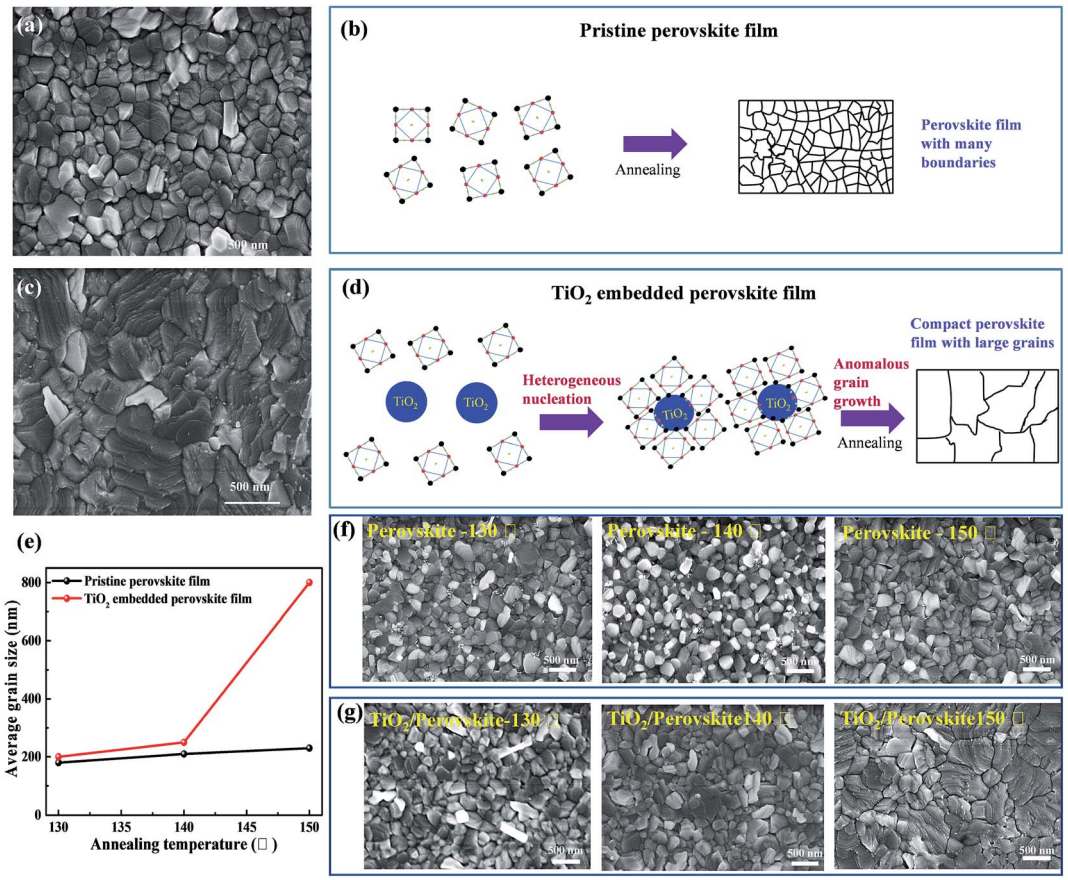

Fig. 4 Scanning electron microscopy (SEM) images of (a) pristine perovskite film (average grain size ~ 200 nm) and (c) TiO_2 embedded perovskite film (0.05 wt% TiO_2 in the TiO_2/PbI_2 blend) (average grain size ~ 800 nm). Schematic illustration of the process of nucleation and growth of perovskite grains (b) without and (d) with TiO_2 nanoparticles. (e) Plots of average grain size *vs.* annealing temperature corresponding to the pristine perovskite films and the embedded TiO_2 films. (f) and (g) present the morphology images of the pristine perovskite films and the TiO_2 embedded perovskite films annealed at temperatures of 130 °C, 140 °C and 150 °C, respectively.

leading to the perovskite grains in the embedded perovskite film yielding many reentrant edges which can promote the grain growth,[18] as shown in Fig. S2.†

In the anomalous grain growth process, the annealing process plays a very important role to drive the mobility of the grain boundaries. With the annealing proceeding to a relatively high temperature, the boundaries of the embedded grains will migrate and a number of small grains grow and infiltrate into each other.[20] Hence, the grain size is greatly increased, leading to the large grain size of the embedded perovskite film, as shown in Fig. 4d. This anomalous grain growth process induced by the existence of TiO_2 nanoparticles can be confirmed by the change of the perovskite grain size with the annealing temperature, as shown in Fig. 4e–g. In the normal grain growth scenario without TiO_2 nanoparticles, the grain size increases gently with the annealing temperature as expected. In the anomalous grain growth scenario with TiO_2 nanoparticles, the grain size increases abruptly with the temperature, as shown in Fig. 4e and g, the average grain size increases from less than 200 nm to around 800 nm in the TiO_2 embedded perovskite film. The uniform and compact perovskite films with a larger grain size possess less grain boundaries and fewer traps, minimizing the carrier losses induced at the grain boundaries and by the trap states.[21] Thus, the improved morphology of the perovskite films induced by the presence of TiO_2 nanoparticles can be concluded to be one of the main origins of the high performance of the TiO_2 embedded PSCs. In addition, larger grains and the compact morphology of the embedded perovskite film minimize the negative impact of oxygen and moisture, which favors the long-term stability of the corresponding films and devices.

The embedded TiO_2 nanoparticles can enhance the electron extraction properties in the TiO_2 embedded perovskite film as well. Hence, time resolved photoluminescence spectroscopy (TRPL) is employed.[22,23] For better comparison, the pristine perovskite film and the perovskite film on compact TiO_2 are also characterized.

As shown in Fig. 5, PL decay shows stretch-exponential profiles, indicating that the decay is governed by the bimolecular recombination process. The bimolecular recombination rates a ($a = B\Delta n_0$, where B and Δn_0 represent bimolecular recombination coefficient ($cm^3\ s^{-1}$) and the excess carrier concentration (cm^{-3}) at $t = 0$) of the perovskite films can be

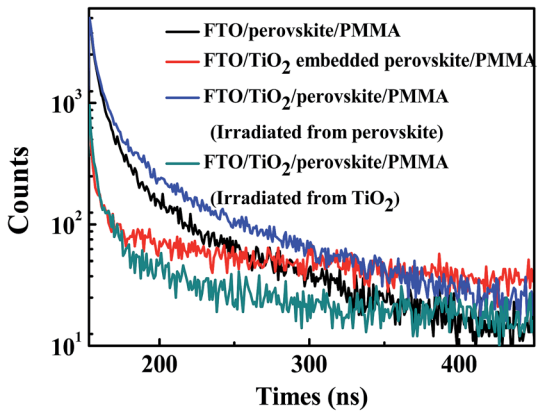

Fig. 5 Time resolved photoluminescence decay at 760 nm obtained for the standard planar perovskite films and for the embedded perovskite films.

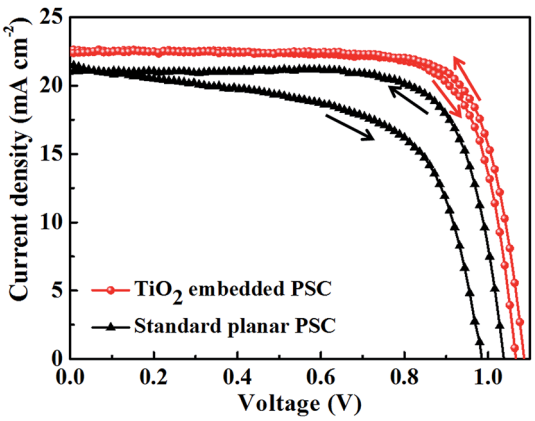

Fig. 6 *J–V* curves of the embedded and the standard planar PSCs obtained from forward scan (from short-circuit to open-circuit) and reverse scan (from open-circuit to short-circuit). The measurements were taken under 1 sun illumination (100 mW cm^{-2}) and at a voltage scan speed of 100 mV s^{-1}.

estimated by fitting the decay curves with the bimolecular recombination equation as follows:

$$I = I_0(1 + at)^{-2} \quad (2)$$

The TiO_2 embedded perovskite film shows a much faster decay with a recombination rate of 2.2×10^8 s^{-1} compared to the pristine perovskite film ($a = 1.2 \times 10^8$ s^{-1}), indicating the extraction of the photo-generated electrons from the perovskite to TiO_2. The perovskite film on compact TiO_2 yields different decay trends depending on the irradiation side. Under conditions of irradiation from the perovskite side, the PL decay profile ($a = 1.1 \times 10^8$ s^{-1}) is similar to that of the pristine perovskite film, pointing to the fact that most of the photo-generated electrons are not extracted from the perovskite to the compact TiO_2 layer, which also implies that the electrons generated inside the perovskite film (away from the compact TiO_2) cannot be extracted effectively. For irradiation from the compact TiO_2 side under which condition the photo-generated electrons move close to the compact TiO_2/perovskite interface, the decay becomes fast with a decay rate of 1.8×10^8 s^{-1}, which is similar to that of the TiO_2 embedded perovskite film. Hence, the TiO_2 embedded structure possesses better electron extraction ability than the compact TiO_2, *i.e.*, the electron extraction is more efficient in the TiO_2 embedded film than in planar perovskite, as shown in Fig. S3.† Furthermore, high resolution transmission electron microscopy (HRTEM, Fig. S4 and S5†) reveals that the perovskite grains are surrounded by the continuous TiO_2 nanoparticles, which form an electron transport network and conduct the electrons to the compact TiO_2 layer. In consequence, the favored electron extraction from perovskite grains to the outer circuit benefits the suppression of carrier recombination in the perovskite film, leading to a low carrier recombination current in the corresponding PSCs.

Furthermore, the TiO_2 embedded PSCs exhibit lower hysteresis than the standard planar PSCs. The *J–V* curves obtained from forward and reverse scans of the optimized embedded PSC and the optimized standard planar PSC are shown in Fig. 6. The forward and the reverse *J–V* curves corresponding to the embedded PSC present less difference compared with those of the standard planar PSC. The low hysteresis of the embedded PSCs can be attributed to the larger grain size of perovskite with fewer trap states and the higher electron extraction efficiency for reduced carrier recombination.[24] In addition, the high-quality grains of the embedded perovskite possess less disordered lattices and can refine the accumulation of unstable ions in the vicinity of grains, resulting in a slower process of electrode polarization.[25] Furthermore, the embedded TiO_2 nanoparticles scattered around the perovskite grains (shown in Fig. S6†) provide many TiO_2/perovskite interfaces which could minimize the effect of the traps of the perovskite surface, resulting in low hysteresis.

The stability of the perovskite films and the PSCs in ambient surroundings is the key issue affecting their applications. Here, it is proved that the incorporation of TiO_2 nanoparticles in fabricating perovskite films improves the film and device stability. The pristine and embedded perovskite films were degraded in ambient air (temperature: 21 °C; humidity: 40%) for 21 days, and their absorption spectra and digital photos were recorded every 7 days. As shown in Fig. 7a, the absorption profile of the pristine perovskite film varies with the degradation period, demonstrating the gradual decomposition of the pristine perovskite film. In particular, the absorption profile corresponding to the perovskite film degraded for 21 days is similar to that of pure PbI_2, revealing the serious decomposition of the pristine perovskite film. In contrast, the TiO_2 embedded perovskite film presents excellent stability after degradation for 21 days, as shown in Fig. 7b, which only yields small changes in the absorption intensity. The photos of these perovskite films also present a similar changing tendency, *i.e.*, the color of the pristine film changed from dark-red to light-yellow whereas the TiO_2 embedded film shows no obvious change after a long period of degradation (21 days). In addition, X-ray diffraction (XRD) measurement was employed as well, as shown in Fig. S7(a and b).† Comparing the XRD patterns of the pristine

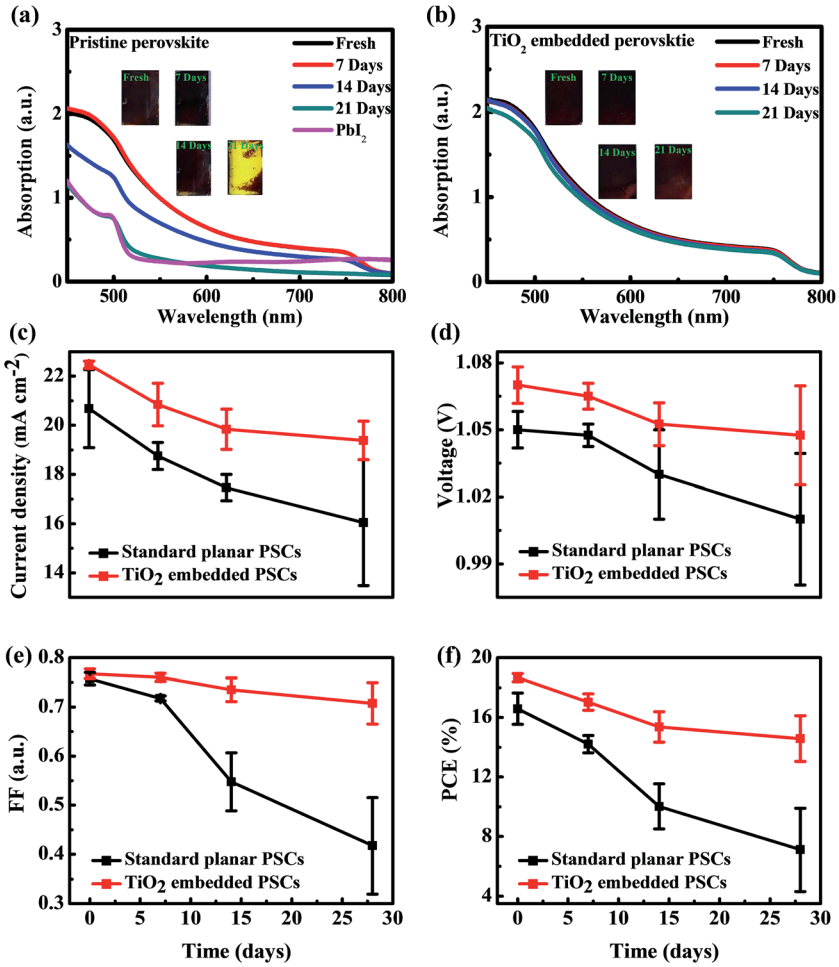

Fig. 7 The absorption spectra of (a) pristine perovskite film and (b) TiO_2 embedded perovskite film (0.05 wt% TiO_2 in the TiO_2/PbI_2 blend) *versus* the degradation time. Insets are the digital photos of these films. The absorption measurement and the photos were taken every 7 days. (c–f) Photovoltaic parameters ((c) J_{SC}. (d) V_{OC}. (e) FF. (f) PCE) of the standard planar PSCs and the TiO_2 embedded PSCs *versus* the degradation period in ambient air. These PSCs were measured every 7 days and stored in ambient air (kept in the dark) before and after *J–V* measurement.

perovskite film and the TiO_2 embedded perovskite film, it is clear that the pristine perovskite film shows a more intense diffraction peak of PbI_2 than the embedded perovskite film after being stored in ambient air for 28 days, again demonstrating that the embedded perovskite film possesses stronger tolerance to ambient air.

Furthermore, the stability of the embedded PSCs is also improved. In order to eliminate the influence of the HTM/metal interface on the stability of perovskite solar cells,[15] we studied the stability of perovskite solar cells by a non-persistent measuring method by measuring these planar and TiO_2 embedded PSCs every 7 days, keeping these devices in the dark before and after *J–V* measurement. The photovoltaic parameters *versus* degradation time are presented in Fig. 7c–f, which reveals that the embedded PSCs degrade slower than the standard planar PSCs. J_{SC} and FF of the embedded PSCs are obviously better than those of the standard planar PSCs. Hence, the average PCE of the embedded PSC exhibits excellent long-term stability, which approaches 80% of the initial average PCE over 28 days. In comparison, the average PCE of the standard planar PSC is degraded almost 40% for the same period. These results reveal that the TiO_2 embedded structure can significantly enhance the long-term stability of PSCs. The excellent long-term stability of the perovskite films and devices with the TiO_2 embedded structure is benefited from the embedded TiO_2 nanoparticles. Previous studies reveal that the PSCs with large perovskite grains and a compact perovskite film possess better device stability,[26,27] because large grains and the compact film can minimize the negative impact of oxygen and moisture. In the presence of TiO_2 nanoparticles, the perovskite films are compact and yield a large grain size (as revealed by the SEM images in Fig. S1 in the ESI†), which are beneficial for the device stability. Meanwhile, it is also reported that the PSCs with a TiO_2 mesoporous scaffold present better stability than the planar PSCs, because the film formation and the coverage of PSCs with the TiO_2 mesoporous structure can be well controlled by the scaffold layer.[28,29] Here, the embedded TiO_2 plays a similar role as the TiO_2 scaffold, which can also improve the film performance and coverage, leading to the formation of the compact perovskite film, and hence, leading to better device stability.

Combining the above benefits, the embedded perovskite films and PSCs show improved device stability than the standard planar PSCs.

Conclusions

A smart hybrid structure of TiO_2 embedded perovskite was proposed to take advantage of TiO_2 nanoparticles in perovskite films. The PSCs based on such a hybrid structure as the active layer, defined as the embedded PSCs, possess a different architecture from the reported mesoporous or planar PSCs. The embedded PSCs exhibit excellent photovoltaic performance and long-term stability compared to the standard planar PSCs, owing to the enhanced electron extraction and the enlarged grain size of the perovskite promoted by the TiO_2 nanoparticles. This novel TiO_2 embedded structure provides an optional structure to construct perovskite solar cells and opens up a new path for enhancing the photovoltaic performance and long-term stability of PSCs through a facile way.

Experimental section

Materials

All the materials were purchased from commercial sources and used as received. CH_3NH_3I was purchased from Xi'an Polymer Light Technology Corp. (purity: 99.5%), PbI_2 was purchased from Alfa Aesar (purity: 99.999%) and TiO_2 was purchased from Aladdin. *N*,*N*-Dimethylformamide (DMF) and dimethyl sulfoxide (DMSO) were purchased from Acros Oganics (Extra dry).

Fabrication of $TiO_2/CH_3NH_3PbI_3$ films and PSCs

$TiO_2/CH_3NH_3PbI_3$ films were fabricated using a modified sequential deposition process.[14] For forming TiO_2 embedded $CH_3NH_3PbI_3$ films, TiO_2/PbI_2 was first loaded by spin-coating onto a compact TiO_2 layer from 1 M PbI_2/DMSO solutions containing various amounts of TiO_2 nanoparticles (particle size: 25–30 nm; rutile nanoparticle, as shown in Fig. S8†), and then dipped into a solution of CH_3NH_3I in ultra-dry isopropanol for 5 min, and the $TiO_2/CH_3NH_3PbI_3$ films formed followed by annealing at 150 °C. For obtaining the mixed precursor solution of TiO_2 and PbI_2, TiO_2 nanoparticles (particle size: 25–30 nm) were added into the PbI_2/DMSO solution, which is 0–0.1 wt% in the TiO_2/PbI_2 blend. The TiO_2/PbI_2/DMSO precursor solution was stirred for 5 h to make sure that the TiO_2 nanoparticles were dispersed uniformly in the solution. The CH_3NH_3I/IPA solution with the concentration of 40 mg ml^{-1} was stirred intensely to obtain the well dissolved solution. All of the procedures were carried out in a glovebox filled with high purity N_2. For fabricating PSCs, the compact TiO_2 layer was deposited on the FTO substrate by $TiCl_4$ treatment as illustrated in our previous work,[30] and then the $TiO_2/CH_3NH_3PbI_3$ films containing various amounts of TiO_2 (0–0.1 wt%) were fabricated by a sequential method, and the HTM layer was deposited sequentially. After that, the Au electrode was sputtered.

Characterization

Current–voltage curves were measured using a source meter (Keithley 2400) under AM 1.5G irradiation with a power density of 100 mW cm^{-2} from a solar simulator (XES-301S+EL-100). The morphologies of the as-prepared $CH_3NH_3PbI_3$ with and without TiO_2 nanoparticles were characterized by scanning electron microscopy (SEM) (FEI SIRION 200). The chemical compositions and structures of the films were analyzed by X-ray diffraction (XRD) (Bruker D8 Advance X-ray diffractometer, Cu-Kα radiation $\lambda = 0.15406$ nm).

Acknowledgements

This work is supported partially by the National High-tech R&D Program of China (863 Program, No. 2015AA034601), National Natural Science Foundation of China (Grant no. 91333122, 61204064, 51202067, 51372082, 51402106 and 11504107), Par-Eu Scholars Program, and the Fundamental Research Funds for the Central Universities. N. G. P. acknowledges the financial support from the National Research Foundation of Korea (NRF) grants funded by the Ministry of Science, ICT & Future Planning (MSIP) of Korea under contracts No. NRF-2012M3A6A7054861 (Global Frontier R&D Program on Center for Multiscale Energy System).

References

1 H. S. Kim, C. R. Lee, J. H. Im, K. B. Lee, T. Moehl, A. Marchioro, S. J. Moon, R. Humphry-Baker, J. H. Yum, J. E. Moser, M. Grätzel and N. G. Park, Lead Iodide Perovskite Sensitized All-Solid-State Submicron Thin Film Mesoscopic Solar Cell with Efficiency Exceeding 9%, *Sci. Rep.*, 2012, **2**, 591.

2 D. Bi, W. Tress, M. I. Dar, P. Gao, J. Luo, C. Renevier, K. Schenk, A. Abate, F. Giordano, J. P. Correa Baena, J. D. Decoppet, S. M. Zakeeruddin, M. K. Nazeeruddin, M. Grätzel and A. Hagfeldt, Efficient luminescent solar cells based on tailored mixed-cation perovskites, *Sci. Adv.*, 2016, **2**, e1501170.

3 W. S. Yang, J. H. Noh, N. J. Jeon, Y. C. Kim, S. Ryu, J. Seo and S. I. Seok, High-performance photovoltaic perovskite layers fabricated through intramolecular exchange, *Science*, 2015, **348**, 1234–1237.

4 F. Fu, T. Feurer, T. Jäger, E. Avancini, B. Bissig, S. Yoon, S. Buecheler and A. N. Tiwari, Low-temperature-processed efficient semi-transparent planar perovskite solar cells for bifacial and tandem applications, *Nat. Commun.*, 2015, **6**, 8932.

5 X. Li, M. I. Dar, C. Yi, J. Luo, M. Tschumi, S. M. Zakeeruddin, M. K. Nazeeruddin, H. Han and M. Graetzel, Improved performance and stability of perovskite solar cells by crystal crosslinking with alkylphosphonic acid omega-ammonium chlorides, *Nat. Chem.*, 2015, **7**, 703–711.

6 D. Song, D. Wei, P. Cui, M. Li, Z. Duan, T. Wang, J. Ji, Y. Li, J. M. Mbengue, Y. Li, Y. He, M. Trevor and N. G. Park, Dual function interfacial layer for highly efficient and stable lead

halide perovskite solar cells, *J. Mater. Chem. A*, 2016, **4**, 6091–6097.
7 M. M. Lee, J. Teuscher, T. Miyasaka, T. N. Murakami and H. J. Snaith, Efficient hybrid solar cells based on meso-superstructured organometal halide perovskites, *Science*, 2012, **338**, 643.
8 Q. Chen, H. Zhou, Z. Hong, S. Luo, H. S. Duan, H. H. Wang, Y. Liu, G. Li and Y. Yang, Planar Heterojunction Perovskite Solar Cells *via* Vapor-Assisted Solution Process, *J. Am. Chem. Soc.*, 2014, **136**, 622–625.
9 F. Giordano, A. Abate, J. P. Correa Baena, M. Saliba, T. Matsui, S. H. Im, S. M. Zakeeruddin, M. K. Nazeeruddin, A. Hagfeldt and M. Graetzel, Enhanced electronic properties in mesoporous TiO_2 *via* lithium doping for high-efficiency perovskite solar cells, *Nat. Commun.*, 2016, **7**, 10379.
10 G. Grancini, S. Marras, M. Prato, C. Giannini, C. Quarti, F. De Angelis, M. De Bastiani, G. E. Eperon, H. J. Snaith, L. Manna and A. Petrozza, The Impact of the Crystallization Processes on the Structural and Optical Properties of Hybrid Perovskite Films for Photovoltaics, *J. Phys. Chem. Lett.*, 2014, **5**, 3836–3842.
11 Y. Li, L. Meng, M. Yang, G. Xu, Z. Hong, Q. Chen, J. You, G. Li, Y. Yang and Y. Li, High-efficiency robust perovskite solar cells on ultrathin flexible substrates, *Nat. Commun.*, 2016, **7**, 10214.
12 F. Li, C. Ma, H. Wang, W. Hu, W. Yu, A. D. Sheikh and T. Wu, Ambipolar solution-processed hybrid perovskite phototransistors, *Nat. Commun.*, 2015, **6**, 8238.
13 T. C. Sum and N. Mathews, Advancements in perovskite solar cells: photophysics behind the photovoltaics, *Energy Environ. Sci.*, 2014, **7**, 2518–2534.
14 J. Burschka, N. Pellet, S. J. Moon, R. Humphry-Baker, P. Gao, M. K. Nazeeruddin and M. Grätzel, Sequential deposition as a route to high-performance perovskite-sensitized solar cells, *Nature*, 2013, **499**, 316–319.
15 D. Wei, T. Wang, J. Ji, M. Li, P. Cui, Y. Li, G. Li, J. M. Mbengue and D. Song, Photo-induced degradation of lead halide perovskite solar cells caused by the hole transport layer/metal electrode interface, *J. Mater. Chem. A*, 2016, **4**, 1991–1998.
16 S. S. Li, C. H. Chang, Y. C. Wang, C. W. Lin, D. Y. Wang, J. C. Lin, C. C. Chen, H. S. Sheu, H. C. Chia, W. R. Wu, U. S. Jeng, C. T. Liang, R. Sankar, F. C. Chou and C. W. Chen, Intermixing-seeded growth for high-performance planar heterojunction perovskite solar cells assisted by precursor-capped nanoparticles, *Energy Environ. Sci.*, 2016, **9**, 1282–1289.
17 S. J. Dillon, M. Tang, W. C. Carter and M. P. Harmer, Complexion: A new concept for kinetic engineering in materials science, *Acta Mater.*, 2007, **55**, 6208–6218.
18 B. Lee, S. Chung and S. L. Kang, Grain boundary faceting and abnormal grain growth in $BaTiO_3$, *Acta Mater.*, 2000, **48**, 1575–1580.
19 T. Salim, S. Sun, Y. Abe, A. Krishna, A. C. Grimsdale and Y. M. Lam, Perovskite-based solar cells: impact of morphology and device architecture on device performance, *J. Mater. Chem. A*, 2015, **3**, 8943–8969.
20 W. Rheinheimer and M. J. Hoffmann, Grain growth transitions of perovskite ceramics and their relationship to abnormal grain growth and bimodal microstructures, *J. Mater. Sci.*, 2016, **51**, 1756–1765.
21 H. S. Kim and N. G. Park, Parameters Affecting *I–V* Hysteresis of $CH_3NH_3PbI_3$ Perovskite Solar Cells: Effects of Perovskite Crystal Size and Mesoporous TiO_2 Layer, *J. Phys. Chem. Lett.*, 2014, **5**, 2927–2934.
22 D. Song, P. Cui, T. Wang, D. Wei, M. Li, F. Cao, X. Yue, P. Fu, Y. Li, Y. He, B. Jiang and M. Trevor, Managing Carrier Lifetime and Doping Property of Lead Halide Perovskite by Postannealing Processes for Highly Efficient Perovskite Solar Cells, *J. Phys. Chem. C*, 2015, **119**, 22812–22819.
23 P. W. Liang, C. Y. Liao, C. C. Chueh, F. Zuo, S. T. Williams, X. K. Xin, J. Lin and A. K. Y. Jen, Additive Enhanced Crystallization of Solution-Processed Perovskite for Highly Efficient Planar-Heterojunction Solar Cells, *Adv. Mater.*, 2014, **26**, 3748–3754.
24 O. Almora, I. Zarazua, E. Mas-Marza, I. Mora-Sero, J. Bisquert and G. Garcia-Belmonte, Capacitive Dark Currents, Hysteresis, and Electrode Polarization in Lead Halide Perovskite Solar Cells, *J. Phys. Chem. Lett.*, 2015, **6**, 1645–1652.
25 W. Peng, L. Wang, B. Murali, K. Ho, A. Bera, N. Cho, C. F. Kang, V. M. Burlakov, J. Pan, L. Sinatra, C. Ma, W. Xu, D. Shi, E. Alarousu, A. Goriely, J. H. He, O. F. Mohammed, T. Wu and O. M. Bakr, Solution-Grown Monocrystalline Hybrid Perovskite Films for Hole-Transporter-Free Solar Cells, *Adv. Mater.*, 2016, **28**, 3383–3390.
26 J. A. Christians, P. A. M. Herrera and P. V. Kamat, Transformation of the Excited State and Photovoltaic Efficiency of $CH_3NH_3PbI_3$ Perovskite upon Controlled Exposure to Humidified Air, *J. Am. Chem. Soc.*, 2015, **137**, 1530–1538.
27 L. C. Smith, E. T. Hoke, D. Solis-Ibarra, M. D. McGehee and H. I. Karunadasa, A layered hybrid perovskite solar-cell absorber with enhanced moisture stability, *Angew. Chem., Int. Ed.*, 2014, **53**, 11232–11235.
28 A. Fakharuddin, F. Di Giacomo, I. Ahmed, Q. Wali, T. M. Brown and R. Jose, Role of morphology and crystallinity of nanorod and planar electron transport layers on the performance and long term durability of perovskite solar cells, *J. Power Sources*, 2015, **283**, 61–67.
29 N. J. Jeon, J. H. Noh, W. S. Yang, Y. C. Kim, S. Ryu, J. Seo and S. I. Seok, Compositional engineering of perovskite materials for high-performance solar cells, *Nature*, 2015, **517**, 476.
30 P. Cui, P. Fu, D. Wei, M. Li, D. Song, X. Yue, Y. Li, Z. Zhang, Y. Li and J. M. Mbengue, Reduced surface defects of organometallic perovskite by thermal annealing for highly efficient perovskite solar cells, *RSC Adv.*, 2015, **5**, 75622–75629.

